Catalytic Mechanism of the Arylsulfatase Promiscuous Enzyme from Pseudomonas Aeruginosa

ARTICLE *in* CHEMISTRY · JANUARY 2013

Impact Factor: 5.93

CITATIONS
4

READS
56

3 AUTHORS:

Tiziana Marino
Università della Calabria
108 PUBLICATIONS **1,433** CITATIONS
SEE PROFILE

Nino Russo
Università della Calabria
512 PUBLICATIONS **7,941** CITATIONS
SEE PROFILE

Marirosa Toscano
Università della Calabria
199 PUBLICATIONS **3,700** CITATIONS
SEE PROFILE

DOI: 10.1002/chem.201201943

Catalytic Mechanism of the Arylsulfatase Promiscuous Enzyme from *Pseudomonas Aeruginosa*

Tiziana Marino,* Nino Russo, and Marirosa Toscano[a]

Abstract: To elucidate the working mechanism of the "broad substrate specificity" by the *Pseudomonas aeruginosa* aryl sulfatase (PAS) enzyme, we present here a full quantum chemical study performed at the density functional level. This enzyme is able to catalyze the hydrolysis of the original *p*-nitrophenyl-sulfate (PNPS) substrate and the promiscuous *p*-nitrophenyl-phosphate (PNPP) one with comparable reaction kinetics. Based on the obtained results, a multistep mechanism including activation of the nucleophile, the nucleophilic attack, and the cleavage of the S–O (P–O) bond is proposed. Regarding the phosphate monoester, the results indicate that only some steps of the promiscuous reaction are identical to those in the native process. Differences concern mainly the last step in which the His115 residue acts as a general base to accept the proton by the O atom of the FGly51 in the PNPS, whereas in PNPP, the Asp317 protonated residue works as a general acid to deliver a proton by a water molecule to the oxygen atom of the C–O bond. The shapes of the relative potential- energy surface (PES) are similar in the two examined cases but the rate-determining step is different (nucleophile attack vs. nucleophile activation). The influence of the dispersion contributions on the investigated reactions was also taken into account.

Keywords: catalysis · density functional theory · enzymes · kinetics · PAS

Introduction

In the last decades broad reaction specificity was found in the biocatalysis field in which enzymes can catalyze alternate reactions. This behavior, known as catalytic promiscuity, consists in the ability of the enzymes to enhance the rate of distinct chemical reactions based on the formation or breaking of different types of bonds. Several advantages arise from this particular activity in an enzyme. In fact, common mechanistic features can be utilized in various chemical transformations and help us to understand, for example, how the modifications of particular catalytic groups can generate different outcomes or provide the improvement of the reaction rate and specificities of enzymes by means of a comparison between cognate and promiscuous reactions mechanisms.[1–8]

Many biological molecules contain phosphate or sulfate and the related enzymatic transformations play eminent roles in the metabolism processes. For example, esterification with sulfate can be useful to solubilize molecules facilitating their excretion or aiding in transport as emerged for sulfate monoesters found among many classes of natural products.

Sulfatases (EC: 3.1.6) represent a class of enzymes involved in the hydrolysis of sulfate ester bonds in a variety of structurally different compounds ranging from complex glucosaminoglucans and glycolipids to sulfated hydroxyl steroids and amino acids.[9]

The *Pseudomonas aeruginosa* arylsulfatase (PAS) is a sulfate monoester hydrolase that uses an unusual amino acid modification to generate the nucleophile species in the active site: the hydrated form of the Cα-formylglycine residue 51 (FGly). This residue is post-translationally generated by the oxidation of a conserved cysteine in prokaryotic and eukaryotic sulfatases and represents the key catalytic residue in the bacterial PAS and corresponds to residues 69 and 91 in the human arylsulfatase A (ASA) and in the arylsulfatase B (ASB), respectively. The fact that the FGly residue is essential for the catalytic activity is reinforced by the alanine and serine mutants that generate a reduction in the catalysis.[10]

PAS was classified as a member of the alkaline phosphatase (AP) superfamily.[11,12] The assignment of this class of sulfatases was done by a combination of different criteria such as sequence and structure or common mechanistic steps. It's known that PAS acts as a sulfatase in vivo by hydrolyzing several aromatic sulfate esters.[13] The promiscuous nature of this enzyme is associated with the fact that a phosphate monoesterase activity was reported,[14] even if this kind of reaction is catalyzed less efficiently than that in vivo. The catalytic proficiencies in terms of $(k_{cat}/K_m)/k_2$ of the enzymatic reactions for sulfate and phosphate are 4.3×10^{18} and 1.6×10^{13}, respectively.[15] As a result of this behavior,

[a] Dr. T. Marino, Prof. N. Russo, Prof. M. Toscano
Department of Chemistry, Università della Calabria
87036 Arcavacata di Rende (Italy)
Fax: (+39) 0984-492044
E-mail: tmarino@unical.it

Supporting information for this article is available on the WWW under http://dx.doi.org/10.1002/chem.201201943.

PAS shows as a cognate activity sulfate monoesterase and as a promiscuous one phosphate monoesterase.

PAS represents the novelty in the field of the hydrolase metalloproteins owing to the fact that it contains the calcium ion in the active center instead of the most usual metal ions (Zn or/and Mg) present in other members of the alkaline phosphatase superfamily.[17]

It's known that the chemistry of sulfate monoesters is mechanistically similar to that of phosphate monoesters, the main difference consists in the total charge. For this reason, although both catalyzed reactions have a hydrolytic nature, intrinsic chemistry can require alternative mechanisms.

In this scenario, our investigation of the working mechanism of the PAS can be useful to evidence the possible mechanistic differences that can justify the different catalytic performances experimentally observed for the hydrolysis of sulfate ester and phosphate monoester. The quantum chemical cluster methodology, in the framework of density functional theory, was applied following a computational procedure well consolidated as evidenced by numerous work devoted to enzyme chemistry.[18–23]

Active-site model: The crystal structure of the bacterial sulfatase from *Pseudomonas aeruginosa* (PAS) determined at 1.3 Å (PDB code: 1HDH)[24] was chosen to build up the cluster model used in our investigation for both sulfate and phosphate monoesterase activity (Figure 1). Both fold and active sites are strikingly similar to those of human sulfatases. In fact, the starting geometry for our study presents in the active site a noncovalently bonded sulfate that occupies the same position as in the previously isolated *para*-nitrocatecholsulfate complexes.[10,16]

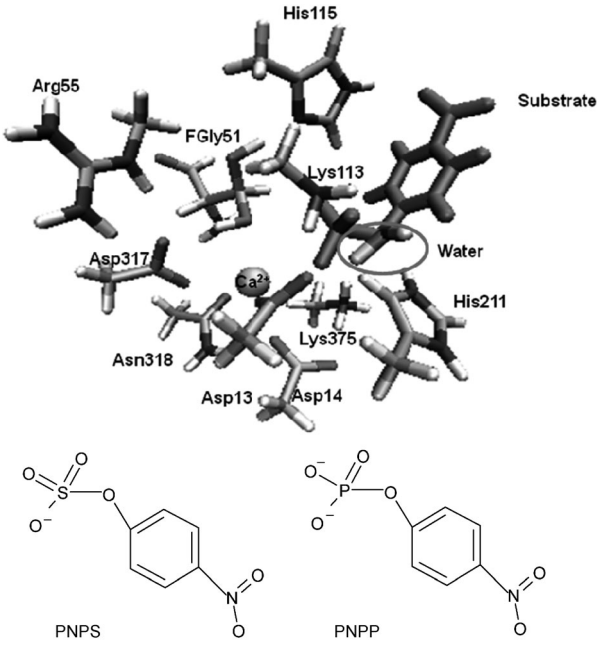

Figure 1. Active-site model of PAS used in this work along with the considered substrates.

The modest resolution in the available structural data for human sulfatases[25,26] led us not to use the relative crystallographic coordinates. Instead, we thought that the model arising from the bacterial arylsulfatase[24] used to study its catalytic mechanism could be also extended to the human one, owing to the fulfilling parallel roles of amino acids occupying equivalent positions in the structures of PAS, ASA, and ASB as shown by kinetic studies with active-site mutants.[10,16,24–26]

In particular, the model consists of a calcium ion the ligands of which in the first coordination shell are Asp13, Asp14, Asp317, Asn318, FGly51, and 4-nitronitrophenyl sulfate. Other important second shell residues, such as His115, His 211, Lys113, Lys375, and Arg55, were included in the model. A water molecule not directly bound to the calcium ion but belonging to its outer coordination sphere was added, in view of its likely role in the catalytic reaction. Hydrogen atoms were added manually, and all the amino acids in the model were truncated so that only side chains were conserved. In particular, histidines were simulated by imidazoles, aspartate by acetate, lysine by methylamine, asparagine by acetamide, and arginine by *N*-methyl-guanidine. The carbon atoms where truncation was made were frozen to their original X-ray positions to prevent artificial movements during the optimization procedure.

The total charge of the model is +2 and +1 for the sulfate and phosphate systems, respectively. In both cases the total number of atoms is 120.

The presence in the catalytic active site of a large amount of positive charge is very common in the sulfatase and phosphatase family since the presence of Lys and Arg amino acids and a calcium ion offers a region of extraordinarily high positive charge density, which is useful to stabilize the higher negative density present in its cavity increasing also from the oxygen atoms of the substrate molecule. The two substrates *p*-nitrophenyl-sulfate (PNPS) and -phosphate (PNPP) taken into account in this paper are natural for the PAS enzyme as proposed by different work.[1,14,27–29]

Results and Discussion

Sulfate and phosphate monoesters share tetrahedral geometry and both bond angles and lengths are similar.[30] Therefore, the most important difference between the two substrates is their charge that, for pH values of 7 and above, is −1 for sulfate and −2 for phosphate monoesters. The results of our analysis concerning the two substrates will be presented separately. Any differences will be discussed and put in evidence with the aim to determine the structural and electronic features that influence the energetics of the two reactions.

Sulfate monoester (PNPS): Despite the fact that sulfate monoesters are present in different classes of natural products and play important biochemical roles, their chemistry is less familiar with respect to that of the phosphate counter-

part. Most recently, a comparative theoretical investigation of the hydrolysis of *p*-nitrophenyl-sulfate and -phosphate in aqueous solution with the aim of evidencing the eventual differences about the hydrolysis reaction of these two esters was undertaken.[31]

Following the experimental indications concerning the possible catalytic cycle followed by the PAS[10,14–16,24,32] as well as our computations, we propose the mechanism summarized in Scheme 1.

The optimized coordinates of the stationary points along the reaction path catalyzed by PAS are reported in the Supporting Information, whereas the potential-energy profile obtained at both B3LYP and B97D levels of theory is depicted in Figure 2.

The optimized structure of the enzyme active site with the substrate corresponding to the Michaelis complex (**ES**, see the Supporting Information) shows a hexacoordinated metallic center contrary to the X-ray structure in which it is heptacoordinated.[24] In fact, the Asp317 residue is now monocoordinated to the Ca^{2+} ion since the $O_{\delta 2}$ is correctly oriented towards the $O_{\gamma 1}$ of the FGly51 residue (1.819 Å). Thus, the discrepancy between our structure and the corresponding X-ray one is essentially due to the fact that in the crystal structure only a sulfate group that acts as an inhibitor is present (for more details see the Supporting Information).

The hydrated form of the FGly51 residue is the nucleophile agent giving rise to the reaction intermediate, the formation of which is followed by cleavage of the C_β–O bond of the hemiacetal rather than that of the S–O bond, to restore the aldehyde form ready to start the catalytic cycle.

Really, to have a good nucleophile it is necessary to deprotonate the $O_{\gamma 1}$ atom of the aldehyde hydrate present in the reactive species FGly51. This activation (Scheme 1, step 1) occurs by means of the Asp317 residue that, acting as a general base, accepts the proton

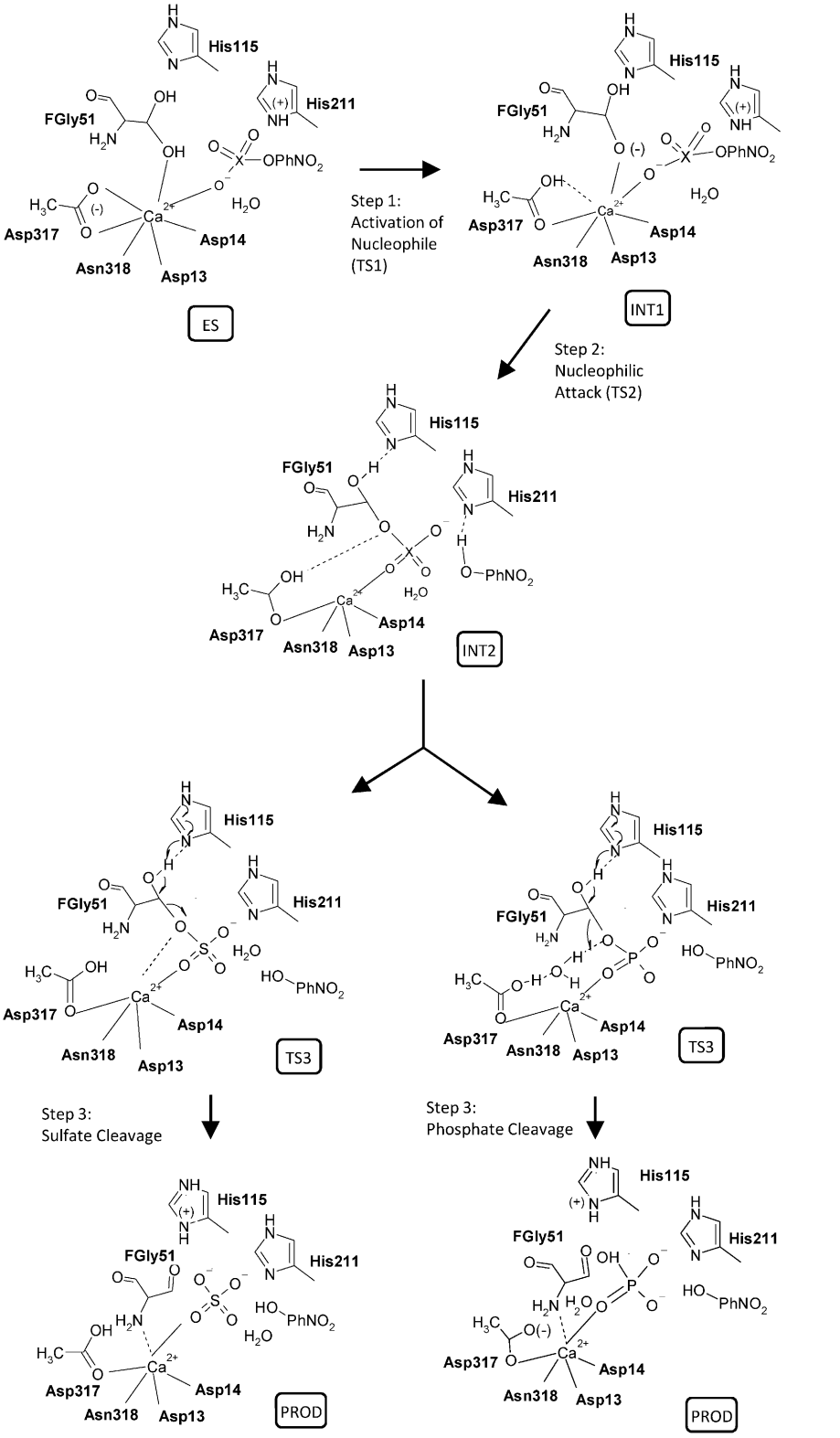

Scheme 1. Suggested mechanism for PNPS and PNPP hydrolase based on the present calculations. For clarity, only the residues implicated in the reaction are shown. For full model see Figure 1

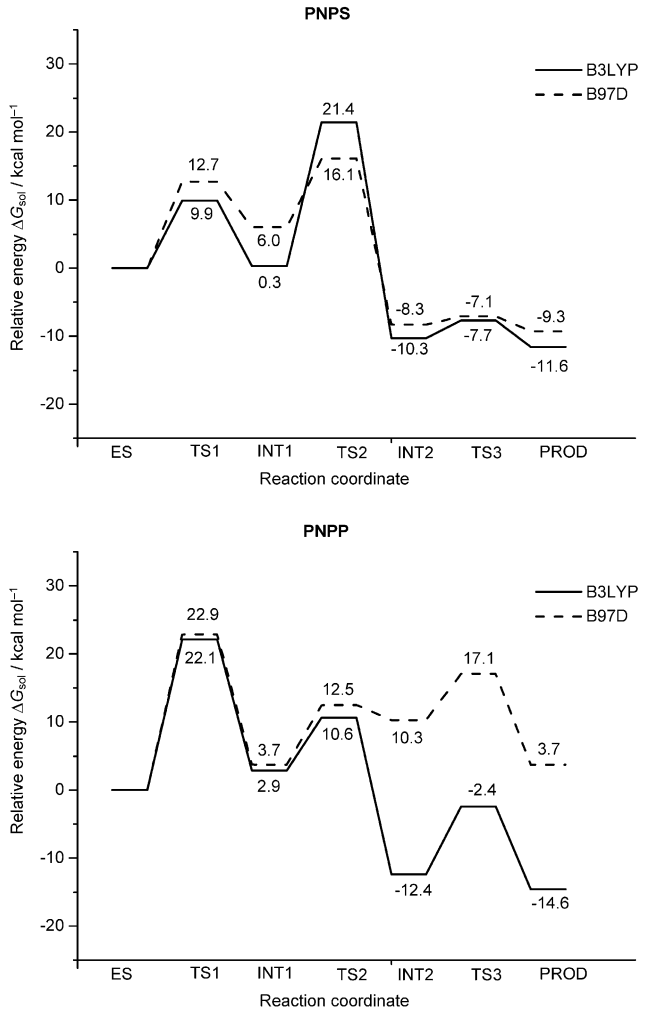

Figure 2. B3LYP (——) and B97D (-----) potential-energy profiles for the mechanism proposed in both PNPS and PNPP substrates examined ($\varepsilon = 4$).

from the hydroxyl $O_{\gamma 1}H$ of FGly51 as is also derived from the experimental evidence.[24] This step is described by **TS1** (Figure 3), which is obtained from **ES** with an expense of 9.9 kcal mol^{-1} (Figure 2). We underline that in the optimized structure the proton shift has already occurred ($O_{\delta 2}H$ Asp317-$O_{\gamma 1}$ FGly51 = 2.136 Å). The imaginary frequency of 278.5*i* cm^{-1} confirms the proton transfer to the carboxylic group of Asp317 coupled with the torsion of the −COOH towards the anionic moiety of Asp13. The new H-bond formed between these two residues will characterize all the following stationary points. The distance between the deprotonated $O_{\gamma 1}$ atom of FGly51 and the sulfur atom is 3.700 Å. The elongation of this distance relative to that present in the crystallographic structure is due to the negative charge density on the deprotonated oxygen atom that, by repulsive forces, induces the exit of the negatively charged sulfate group. The **INT1** is the product of these rearrangements and is almost is energetic with the **ES** (they differ by only 0.3 kcal mol^{-1}, see Figure 2). Now the distance involving the deprotonated $O_{\gamma 1}$ of FGly51 and the sulfur atom is reduced to a value (3.233 Å) that allows the nucleophilic attack.

TS2 is the crucial barrier (21.4 kcal mol^{-1}) to be overcome to carry out the nucleophilic attack from the $O_{\gamma 1}$ ox anion of FGly51 on the sulfate monoester. The obtained structure (Figure 3) suggests that the hydrolysis can proceed in a concerted way. **TS2** is an almost synchronous transition state in which it is possible to observe the formation of the bond between the sulfur atom and the nucleophile (Oγ1-S = 2.265 vs. 3.233 Å in **INT1**) and the breaking of the bond between sulfur atom and the leaving group (S−O_L = 2.074 vs. 1.766 Å in **INT1**). The vibrational analysis confirmed **TS2** as a first-order saddle point the imaginary frequency of which, 226*i* cm^{-1}, correlates well with the stretching mode of the $O_{\gamma 1}$−S and S−O_L bonds.

Natural bond orbital (NBO) analysis gave contributions into the elucidation of the dissociative or associative nature of sulfate monoester hydrolysis. In fact, they showed the presence of a covalent $O_{\gamma 1}$−S bond derived by the overlap between an orbital containing a hybrid sp^3 character on the oxygen atom and one containing a prevalent d character on the sulfur atom. In addition, the analysis indicates the absence of the S−O_L bond. The location of the stationary points in the corresponding More O'Farrell Jencks (MFJ) plot in Figure 4 shows that the hydrolysis of PNPS proceeds through an almost synchronous path.

The S−O_L bond cleavage is accompanied by the shortening of the H-bond involving the leaving group (O_L) and the His211 (1.622 vs. 1.946 Å in **INT1)**. This last event attenuates the incoming negative charge on the oxygen atom of the leaving group that thus is prone to accept the proton from the acid residue (His211) as evidenced by the subsequent intermediate **INT2**. These results match very well with a loose transition state, which is dissociation-like, as also suggested in the literature[14,15,27,32] for the chemistry of sulfate monoesters, in which the sulfuryl group resembles SO_3. The same findings were discovered in various experimental studies.[33–40] The lengthening of the Asp13 Oδ1−Ca^{2+} bond (2.90 vs. 2.42 Å in **ES**) in **TS2** emphasizes the initial reorganization of the inner coordination shell of the calcium ion that, as is well known, in its enzymes can pass through six-, eight-, and seven-ligand coordination with consequent different geometries during the catalytic cycle.[41]

The two Lys residues present in the catalytic cavity provide electrostatic stabilization by means of hydrogen bonds with the negatively charged oxygen atoms of the SO_3 moiety of the penta-coordinated transition state. These positively charged residues play a role similar to that of zinc ions present in the active site of other members of the AP superfamily.[33,42,43]

The product of the nucleophile attack (sulfated protein **INT2**) lies at 13.3 kcal mol^{-1} below the **ES**. From the optimized geometry it's possible to observe the removal of the *p*-nitrophenol (the distance between the O_L and the sulfur atom is 4.729 Å), which, however, remains in the catalytic room owing to the hydrogen bond interaction with His211

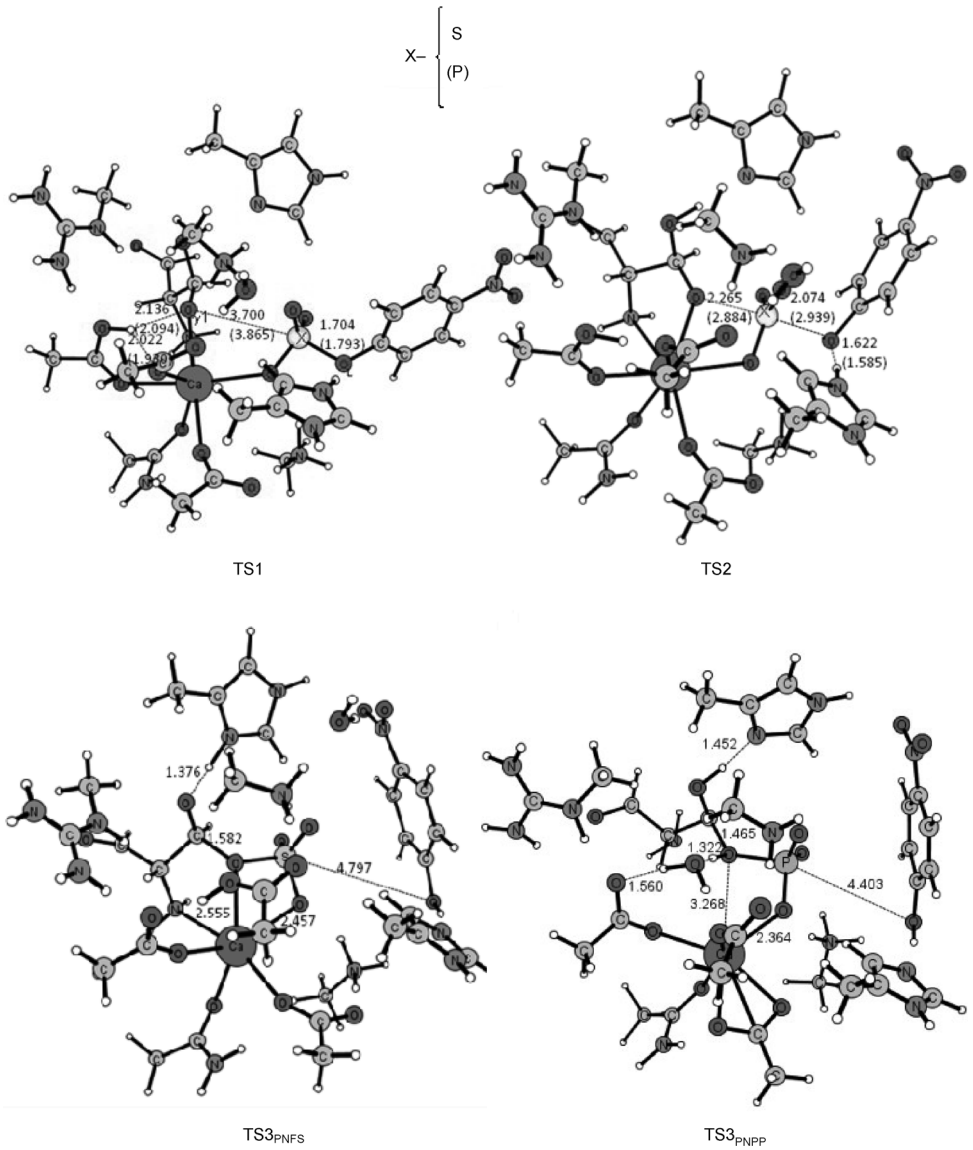

Figure 3. Optimized structures of the transition states (TS1, TS2, and TS3) along the reaction pathway for PNPS and PNPP hydrolase. Distances for the PNPS (PNPP) model are in Å.

(1.619 Å). On the contrary, the FGly51 $O_{\gamma}1$ is bound to the sulfur as evidenced by the relative distance (1.477 Å).

The last step of the mechanism consists in cleavage of the sulfate group to regenerate the aldehyde the formation of which is linked to the breaking of the bond involving the C_{β} atom of FGly51 and the oxygen atom of the sulfate one. To do this, the deprotonation of the alcohol $O_{\gamma 2}$ group in the side chain of FGly51 is required. For this purpose the general base role of the His115 residue is fundamental since it is the most suitable candidate to receive the proton from the alcohol group of FGly51. In fact, the transition state (**TS3** in Figure 3) connecting the **INT2** to the final product **PROD** clearly accounts for this process. The relative barrier is calculated to be only 2.6 kcal mol^{-1} higher than **INT2**. The proton shift from the alcohol $O_{\gamma 2}$ group to the nitrogen atom of His115 gives rise to the lengthening of the C_{β}–O bond that goes from 1.477 (**INT2**) to 1.582 Å. The calculated imaginary frequency of 93*i* cm^{-1} describes the proton transfer to the base and the concomitant C_{β}–O bond cleavage.

The calculations corroborate the fact that the cleavage of the C_{β}–O bond of the hemiacetal form and not the S–O bond represents the final step of the sulfatase hydrolytic path.[14]

The calcium ion retains the same coordination number present in the previous stationary point, and confirms its hard nature as shown by its preference for negatively charged oxygen atoms as donor candidates. The product of S–O bond breaking is the **PROD** species in which the sulfate is coordinated to Ca^{2+} in a bidentate fashion (2.457 and 2.455 Å) and the C_{β}–O distance is 2.483 Å. Asp13 is completely pushed out from the inner coordination shell of the calcium but retained in the catalytic pocket by the hydrogen bond with the Asp317 residue (1.767 Å). The energy of this species is 11.6 kcal mol^{-1} lower than that of the reactant species (**ES**).

The water molecule included in the model acts as a spectator because it does not directly participate in the sulfate monoester hydrolysis reaction.

The introduction of dispersion forces by means of the B97D functional doesn't entail any noticeable influence on the PES, except for the stabilization of the activation barrier (**TS2**) that now is 16.1 kcal mol^{-1} (Figure 2, -----).

Phosphate monoester (PNPP): The catalytic cycle followed in this promiscuous reaction is the same as the native one except for the step of phosphate cleavage (Scheme 1, step 3). The B3LYP and B97D energetic paths are shown in Figure 2, whereas in Figure 3 the transition states located in each step are depicted. The B3LYP-optimized structures of the stationary points are reported in the Supporting Information.

The starting structure of the enzyme–substrate complex containing the phosphate monoester arises from the substitution of the sulfur with the phosphorus in the PNPP. Look-

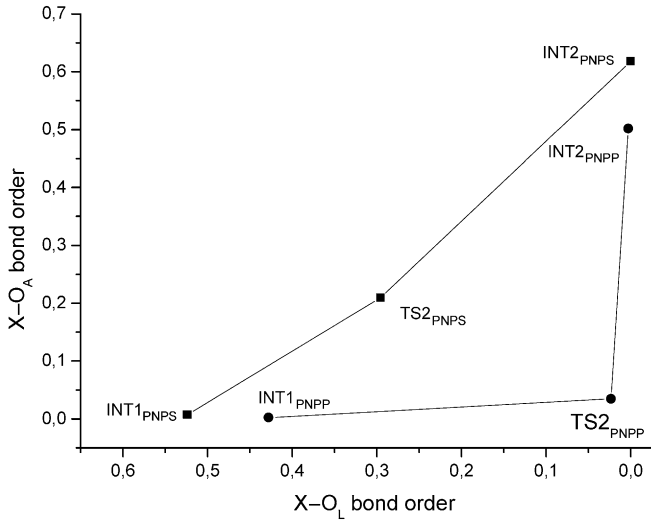

Figure 4. MFJ diagram for the sulfate (PNPS) and phosphate monoester (PNPP) by PAS (X = S for PNPS; X = P for PNPP).

ing at the optimized geometry we note that the main difference in the structure concerns the distance between the oxygen atom of the substrate and the calcium ion. In fact, this distance in the case of PNPP is shorter than that of the PNPS one (2.424 vs. 2.602 Å) as expected by the increase of the negative charge on the oxygen atom (−1.25 vs. −0.75|e|).

As was shown previously, to obtain the species able to perform the nucleophilic attack on the phosphorus atom, a proton transfer from the hydroxyl $O_{\gamma 1}H$ of FGly51 to the carboxylate group of Asp317 is necessary. This occurs throughout **TS1** (Figure 3) with an energy expense of 22.1 kcal mol^{-1}. Contrary to the PNPS case, this process is the rate-determining step. The introduction of a substrate containing a more negative charge causes a consistent change in the charge distribution around the entire active site. The increase of the negative charge on the oxygen atom of Asp317 contributes to the increase of the energy for the proton transfer making this step the rate-determining one.

In the subsequent process the nucleophilic attack, characterized by **TS2**, occurs with a smaller energy request (Figure 2). This kind of concerted transition state represents a loose transition state typical of a phosphomonoester hydrolysis that proceeds through a dissociative or D_NA_N mechanism.[14,15,27,32,44,45] This finding entails that the P–O_L bond is broken before the P–O_{nuc} bond is formed. NBO calculations confirm the absence of the P–O_{nuc} and P–O_L bonds and propose a natural metaphosphate ionlike expansive of **TS2**. It is worth remarking that the NBO calculations supported a more associative nature in the case of the PNPS substrate. Another not negligible factor that reinforces the different behavior of the two considered substrates is the different intensity of the electrostatic interactions established between the two chemical systems and the surroundings that play an important role on the stabilization of **TS2** in the case of the phosphate monoester. In fact, the two Lys residues placed at the sites of the phosphate stabilize it electrostatically. The calculated barrier for **TS2** is 10.6 kcal mol^{-1}, which agrees well with calculated values in similar systems.[17,44,46,47] In confirmation of this, the MFJ plot of Figure 4 clearly proposes a dissociative nature of the PNPP substrate. A semiempirical EVB/MM study mainly devoted to the description of the nucleophilic attack step of PAS on the phosphate monoester found a similar nature in the transition state.[48]

After **TS2**, the reaction goes on by **INT2** in which the phosphate group is chelating the metal ion (2.768 and 2.327 Å). The water molecule is situated between the protonated Asp317 (1.090 Å) and oxygen atom bound to the Cβ atom of the FGly51 (2.535 Å) and is ready to act as a proton shuttle between Asp317 and phosphate. By starting from **INT2** (15.3 kcal mol^{-1} lower than **INT1)**, the last step of the catalytic cycle is exothermic (Figure 2).

Different from what happened in the enzyme with PNPS, in which the C_β–O cleavage is a consequence of the proton shift involving the His115 and the alcohol $O_{\gamma 2}$ group of FGly51, in the PNPP this doesn′t occur, but a water molecule is essential for shuttling the proton from the aspartate residue, which works as a general acid, to the oxygen atom of the phosphate group that must be protonated to move away from the enzyme. Again, this behavior is probably due to the different negative charge present on the two examined substrates. In PNPP all the attempts to describe the Cβ–O bond similarly to what has been done for PNPS have failed. The **TS3** structure accounts for the delivery of the proton from Asp 317 to the oxygen phosphate that in turn gives rise to the proton shift from the alcohol $O_{\gamma 2}$ group of FGly51 to His115 (Figure 3). The distance between the hydrogen atom of the $O_{\gamma 2}$ group of FGly51 and His115 decreases (1.552 Å), the C_β–O bond is elongated from 1.402 (in **INT2**) to 1.465 Å and the proton is 1.103 Å from the oxygen atom of the phosphate. The barrier is 10.0 kcal mol^{-1} above **INT2**.

From this result emerges that for breaking the hemiacetal, the phosphate must be protonated. This fact is not completely weird since the profiles of pH dependence of k_{cat}/K_M for native sulfatase activity toward PNPS and the promiscuous phosphatase activity toward PNPP obtained by Hollfelder et al., showed a dissimilar shape that can be ascribed to eventual "ionization of two enzymatic groups or ionization of one enzymatic group and protonation of the dianion of PNPP ($pK_a = 4.79$)",[14] as proposed by our findings. Furthermore, this conclusion doesn′t invalidate the chemical nature of the reaction characterizing the last step of the working cycle of PAS because it differs only in the leaving group. For the rest, the general acid–base catalysis of the Cβ–O bond cleavage and not the S–O or P–O bond cleavage, is the same for both native and promiscuous reactions. The theoretical study performed in solution on the same two uncatalyzed reactions hypothesized an analoguous behaviour.[31]

The result of **TS3** is the **PROD** that lies at 14.6 kcal mol^{-1} below the **ES** species (Figure 2). It can be observed that the

phosphate is coordinated to Ca^{2+} in an asymmetric bidentate way (2.680 and 2.420 Å) and the C_β–O distance is 2.728 Å. Contrary to the PNPS native substrate, the Asp13 is retained in the inner coordination shell and the calcium ion assumes a heptacoordination as in the X-ray structure.[24]

On the basis of our results we can hypothesize that the hydrolysis of diester phosphate can proceed with improved kinetics due to the fact that the product of the hydrolysis in this reaction shows a charge different from that carried by the PNPS, so probably the last step describing the hemiacetal cleavage will occur in the same way observed in the case of the PNPS substrate. This fact could justify what is observed in the promiscuous phosphodiesterase activity for PAS.[15]

Taking into account the effects of dispersion forces (Figure 2, -----) no remarkable influence is observed in the activation of nucleophile and nucleophilic attack steps, whereas the destabilization of the species involved in the step of phosphate cleavage leads to a profile at higher energy than that obtained at the B3LYP level, but without changing the rate-determining step, which remains **TS1**.

Conclusion

The main structural and energetic characteristics of the proposed catalytic mechanism for the promiscuous substrate recognition by the arylsulfatase promiscuous enzyme from *Pseudomonas aeruginosa*, coming from our density functional theory investigation, can be summarized as follows:

1) The addition–elimination reaction occurs in an almost synchronous way as described by the trigonal bipyramidal transition-state (**TS2**) for both substrates examined and as confirmed by the absence of a stable pentacoordinated intermediate along the reaction pathway. In particular, both NBO analysis and the MFJ plot suggest that the phosphate monoester hydrolysis has a clearly more dissociative character than that of the sulfate.
2) For the phosphate monoester, we found that in this multistep reaction, only some steps of the promiscuous reaction are identical to those in the native reaction.
3) In the case of the PNPP substrate, the Asp317 functions as a general acid to deliver a proton to the oxygen phosphate by means of a water molecule. Previous theoretical and experimental discussions hypothosize a different protonation requirement for the two substrates.
4) Notwithstanding that the general acid–base catalysis involves different acid–base pairs in the two PNPS and PNPP substrates, the evolution of the intermediate towards product involves the same C_β–O bond.
5) In both substrates the leaving group is protonated and stabilized by a hydrogen interaction with His211.
6) Calculations in the protein environment suggest that the rate-determining step is the nucleophilic attack for the PNPS and the nucleophile activation for the PNPP.
7) The introduction of dispersion effects by means of B97D does not introduce noticeable consequences on the PES of PNPS, whereas in the PES of PNPP, the portion describing the phosphate cleavage undergoes an appreciable change due to the different mechanism followed.
8) The different charge distribution induced by the two substrates has a significant effect on the mechanism and on the energetics of the reactions.
9) Comparison of the calculated $\Delta\Delta G$ between two reactions (0.7 kcal mol^{-1}) with that obtained converting to barriers the available experimental kinetic data (1.6 kcal mol^{-1}, applying classical transition-state theory) at the same temperature ($T = 298.15$ K) is satisfactory.

Experimental Section

Computational methods: The Gaussian 03 program package[49] was used for the calculations. Geometry optimizations of all the examined species were carried out by using the B3LYP[50,51] exchange-correlation functional. An all-electron-differentiated basis set scheme was used for all atoms except for the calcium ion which was treated by the LANL2DZ[52] pseudopotential. For sulfur (phosphorus) atoms and the atoms directly implicated in all steps of the catalytic reaction we have used the 6-311+G(2d) basis set, whereas the 6-31G(d,p) description was employed for the remaining atoms. Energies were recalculated by performing single-point calculations with the more extended 6-311+G(2d,2p) basis set for C, N, O, S, and H elements by using still the LANL2DZ pseudopotential for the metal ion.

Vibrational frequencies were calculated at the same level of theory as the optimizations to have zero-point corrections to the energies (ZPE) and to confirm the nature of the stationary points encountered on the potential-energy surfaces. As will be discussed below, some atoms of the considered model were frozen to their X-ray original positions during the optimization procedure. As previously demonstrated, this strategy implicates that the calculation can generate few small imaginary frequencies but, owing to their small values (from 5i to 30i cm^{-1}), these do not influence the ZPE and can be ignored.[53,54] Furthermore, the probable differences in the description of energetics arising from the use of this approach that makes the system slightly rigid, do not alter the conclusions about the followed mechanism.[53–55]

The NBO analysis was performed also to calculate the Wiberg bond orders helpful in clarifying the dissociative or associative nature of the hydrolysis step.[56] The MFJ plot was also considered.[57]

To estimate the effects of the protein environment, the polarizable continuum model (PCM)[58,59] with the dielectric constant value equal to 4, was used by performing single-point calculations with the larger basis set on the optimized gas-phase B3LYP structures. The choice of this dielectric constant value is due to the fact that it is commonly used to simulate the natural surroundings for a protein in quantum-chemical modeling of enzymatic reactions.[60,61] Furthermore to evaluate the effects of the long-range interactions on the reactions catalyzed by the PAS, single-point computations in the protein environment (with the large basis set) on the previous optimized structures were carried out by using the B97D functional including the empirical dispersion correction as proposed by Grimme.[62,63]

Reaction Gibbs free energies in solution, ΔG_{sol}, were calculated for each process as the sum of two contributions: a gas-phase reaction free energy, ΔG_{gas}, and a solvation reaction free energy term calculated with the continuum approach, ΔG_{solv}. The calculated free energies, G, are obtained at $T = 298.15$ K.

Acknowledgements

The University of Calabria, CASPUR, and the MIUR (PRIN 2008F5A3AF 005) are gratefully acknowledged.

[1] I. Catrina, P. J. O'Brien, J. Purcell, I. Nikolic-Hughes, J. G. Zalatan, A. C. Hengge, D. Herschlag, *J. Am. Chem. Soc.* **2007**, *129*, 5760–5765.
[2] R. A. Jensen, *Annu. Rev. Microbiol.* **1976**, *30*, 409–425.
[3] P. J. O'Brien, D. Herschlag, *Chem. Biol.* **1999**, *6*, R91–R105.
[4] D. R. J. Palmer, J. B. Garrett, V. Sharma, R. Meganathan, P. C. Babbitt, J. A. Gerlt, *Biochemistry* **1999**, *38*, 4252–4258.
[5] T. M. Penning, J. M. Jez, *Chem. Rev.* **2001**, *101*, 3027–3046.
[6] S. D. Copley, *Curr. Opin. Chem. Biol.* **2003**, *7*, 265–272.
[7] James LC, Tawfik DS. (2003) Conformational diversity and protein evolution -a 60-year-old hypothesis revisited *Trends BioChem. Sci* 28, 361–368.
[8] O. Khersonsky, C. Roodveldt, D. S. Tawfik, *Curr. Opin. Chem. Biol.* **2006**, *10*, 498–508.
[9] B. Schmidt, T. Selmer, A. Ingendoh, K. von Figura, *Cell* **1995**, *82*, 271–278.
[10] R. von Bülow, B. Schmidt, T. Dierks, K. Von Figura, I. Uson, *J. Mol. Biol.* **2001**, *305*, 269–277.
[11] M. Y. Galperin, A. Bairoch, E. V. Koonin, *Protein Sci.* **1998**, *7*, 1829–1835.
[12] M. Galperin, M. J. Jedrzejas, *Proteins* **2001**, *45*, 318–324.
[13] S. Beil, H. Kehrli, P. James, W. Staudenmann, A. M. Cook, T. Leisinger, M. A. Kertesz, *Eur. J. Biochem.* **1995**, *229*, 385–394.
[14] L. F. Olguin, S. E. Askew, A. C. O'Donoghue, F. Hollfelder, *J. Am. Chem. Soc.* **2008**, *130*, 16547–16555.
[15] A. C. Babtie, S. Bandyopadhyay, L. F. Olguin, F. Hollfelder, *Angew. Chem.* **2009**, *121*, 3746–3749; *Angew. Chem. Int. Ed.* **2009**, *48*, 3692–3694.
[16] M. Chruszcz, P. Laide, M. Monkiewicz, E. Ortlund, L. Lebioda, K. Lewinski, *J. Inorg. Biochem.* **2003**, *96*, 386–392.
[17] M. E. Alberto, T. Marino, N. Russo, M. J. Ramos, *J. Chem. Theory Comput.* **2010**, *6*, 2424–2433.
[18] O. Amata, T. Marino, N. Russo, M. Toscano, *J. Am. Chem. Soc.* **2009**, *131*, 14804–14811.
[19] O. Amata, T. Marino, N. Russo, M. Toscano, *Phys. Chem. Chem. Phys.* **2011**, *13*, 3468–3477.
[20] O. Amata, T. Marino, N. Russo, M. Toscano, *J. Am. Chem. Soc.* **2011**, *133*, 17824–17831.
[21] S.-L. Chen, T. Marino, W.-H. Fang, N. Russo, F. Himo, *J. Phys. Chem. B* **2008**, *112*, 2494–2500.
[22] M. J. Ramos, P. A. Fernandes, *Acc. Chem. Res.* **2008**, *41*, 689–698.
[23] M. Leopoldini, N. Russo, M. Toscano, M. Dulak, T. Wesolowski, *Chem. Eur. J.* **2006**, *12*, 2532–2541.
[24] I. Boltes, H. Czapinska, A. Kahnert, R. von Bülow, T. Dierks, B. Schmidt, K. von Figura, M. A. Kertesz, I. Usón, *Structure* **2001**, *9*, 483–491.
[25] G. Lukatela, N. Krauss, K. Theis, T. Selmer, V. Gieselmann, K. von Figura, W. Saenger, *Biochemistry* **1998**, *37*, 3654–3664.
[26] C. S. Bond, P. R. Clements, S. J. Ashby, C. A. Collyer, S. J. Harrop, J. J. Hopwood, J. M. Guss, *Structure* **1997**, *5*, 277–289.
[27] J. G. Zalatan, D. Herschlag, *J. Am. Chem. Soc.* **2006**, *128*, 1293–1303.
[28] A. Waldow, B. Schmidt, T. Dierks, R. von Buölow, K. von Figura, *J. Biol. Chem.* **1999**, *274*, 12284–12288.
[29] S. Jonas, F. Hollfelder, *Pure Appl. Chem.* **2009**, *81*, 731–742.
[30] P. J. O'Brien, D. Herschlag, *J. Am. Chem. Soc.* **1998**, *120*, 12369–12370.
[31] S. C. L. Kamerlin, *J. Org. Chem.* **2011**, *76*, 9228–9238.
[32] W. W. Cleland, A. C. Hengge, *Chem. Rev.* **2006**, *106*, 3252–3278.
[33] S. J. Benkovic, P. A. Benkovic, *J. Am. Chem. Soc.* **1966**, *88*, 5504–5511.
[34] E. J. Fendler, J. H. Fendler, *J. Org. Chem.* **1968**, *33*, 3852–3859.
[35] N. Bourne, A. Hopkins, A. Williams, *J. Am. Chem. Soc.* **1985**, *107*, 4327–4331.
[36] P. D'Rozario, R. L. Smyth, A. Williams, *J. Am. Chem. Soc.* **1984**, *106*, 5027–5028.
[37] A. Hopkins, R. A. Day, A. Williams, *J. Am. Chem. Soc.* **1983**, *105*, 6062–6070.
[38] R. H. Hoff, P. Larsen, A. C. Hengge, *J. Am. Chem. Soc.* **2001**, *123*, 9338–9344.
[39] B. T. Burlingham, L. M. Pratt, E. R. Davidson, V. J. J. Shiner, J. Fong, T. S. Widlanski, *J. Am. Chem. Soc.* **2003**, *125*, 13036–13037.
[40] C. L. L. Chai, T. W. Hepburn, G. Lowe, *J. Chem. Soc. Chem. Commun.* **1991**, 1403.
[41] C. Andreini, I. Bertini, G. Cavallaro, G. L. Holliday, J. M. Thornton, *J. Biol. Inorg. Chem.* **2008**, *13*, 1205–1218.
[42] S. R. Hanson, M. D. Best, C. H. Wong, *Angew. Chem. Int. Ed.* **2004**, *43*, 5736–5763.
[43] S. Jonas, B. van Loo, M. Hyvönen, F. Hollfelder, *J. Mol. Biol.* **2008**, *384*, 120–136.
[44] V. López-Canut, M. Roca, J. Bertrán, V. Molíner, I. Tuñón, *J. Am. Chem. Soc.* **2011**, *133*, 12050–12062.
[45] S. C. L. Kamerlin, J. Florián, A. Warshel, *ChemPhysChem* **2008**, *9*, 1767–1773.
[46] R.-Z. Liao, J.-G. Yu, F. Himo, *Inorg. Chem.* **2010**, *49*, 6883–6888.
[47] J. G. Zalatan, T. D. Fenn, A. T. Brunger, D. Herschlag, *Biochemistry* **2006**, *45*, 9788–9803.
[48] J. Luo, B. van Loo, S. C. L. Kamerlin, *Proteins Struct. Funct. Bioinf.* **2012**, *80*, 1211–1226.
[49] M. J. Frisch, et al. *Gaussian 03*; Gaussian, InC, Pittsburgh, PA, **2003**.
[50] A. D. J. Becke, *J. Chem. Phys.* **1993**, *98*, 5648–5652.
[51] C. T. Lee, W. T. Yang, R. G. Parr, *Phys. Rev. B* **1988**, *37*, 785–789.
[52] P. J. Hay, W. R. Wadt, *J. Chem. Phys.* **1985**, *82*, 270–283.
[53] P. E. M. Siegbahn, F. Himo, *Comput. Mol. Sci.* **2011**, *1*, 323–336.
[54] S.-L. Chen, W.-H. Fang, F. Himo, *Theor. Chem. Acc.* **2008**, *120*, 515–522.
[55] R.-Z. Liao, J.-G. Yu, F. Himo, *Proc. Natl. Acad. Sci. USA* **2010**, *107*, 22523–22527.
[56] E. D. Glendening, A. E. Reed, J. E. Carpenter, F. Weinhold NBO, version 3.1.
[57] a) W. P. Jencks, *Chem. Rev.* **1985**, *85*, 511–527; b) R. A. More O'Ferrall, *J. Chem. Soc. B* **1970**, 274–277.
[58] V. Barone, M. Cossi, *J. Phys. Chem. A* **1998**, *102*, 1995–2001.
[59] M. Cossi, N. Rega, G. Scalmani, V. Barone, *J. Comput. Chem.* **2003**, *24*, 669–681.
[60] P. E. M. Siegbahn, M. R. A. Blomberg, *Chem. Rev.* **2000**, *100*, 421–438.
[61] L. Noodleman, T. Lovell, W. G. Han, J. Li, F. Himo, *Chem. Rev.* **2004**, *104*, 459–508.
[62] S. Grimme, *J. Comput. Chem.* **2006**, *27*, 1787–1799.
[63] S. Grimme, J. Antony, S. Ehrlich, H. Krieg, *J. Chem. Phys.* **2010**, *132*, 154104.

Received: June 1, 2012
Revised: November 6, 2012
Published online: December 28, 2012

